Structural studies of Sn_x-Sb_{15}-Se_{85-x} chalcogenide glasses

A. B. Adam[1], S. Sakrani[2] & Y. Wahab[2]
[1]*Department of Electrical and Electronics Engineering, Universiti Teknologi PETRONAS, Malaysia*
[2]*Department of Physic, Faculty of Science, Universiti Teknologi, Malaysia*

Abstract

Glass formation tendency has been studied for five different compositions of the Sn_x-Sb_{15}-Se_{85-x} system, where x = 0, 5, 10, 12.5, and 15-mole %. Melt quench-synthesised samples have been characterised using a variety of experimental techniques, including X-ray diffraction (XRD), Fourier transform infrared spectroscopy (FTIR), Raman spectroscopy, differential thermal analysis (DTA), and density measurement. The XRD analysis for x = 0 up to 12.5-mole % gave an indication of amorphous phase, while for x = 15-mole %, it showed a tendency of crystalline structure. The results obtained from FTIR showed a shift in IR-peak intensities and widths from the long to the short wavelengths upon the addition of Sn-mole %. This change implied the breaking of Se-chains that appeared around 208-250 cm^{-1} as well as the occurrence of pyramidal $SbSe_3$ and asymmetrical tetrahedral $SnSe_4$ modes around 176-208 $cm^{-1}$and 125-145 cm^{-1}, respectively. In addition, Raman spectra revealed a pyramidal $SbSe_3$ peak located at 190 cm^{-1}. The intensity of this peak increased and shifted to183 cm^{-1} when Sn-mole % was added to the system. Differential thermal analysis revealed that the glass transition temperature decreased with an increase of Sn-mole %. The results confirmed the validity of using 4, 3, and 2 co-ordination numbers of Sn, Sb, and Se, respectively, in the amorphous samples.

Keywords: XRD, DTA, FTIR, Raman, Sn-Sb-Se-chalcogenide glasses.

1 Introduction

One of the most challenging contemporary problems for structural materials science is the collection of sufficiently comprehensive experimental data sets

WIT Transactions on The Built Environment, Vol 97, © 2008 WIT Press
www.witpress.com, ISSN 1743-3509 (on-line)
doi:10.2495/HPSM080501

from complementary probe techniques. The purpose of this is to be able to describe accurately and unambiguously the structure of amorphous materials and follow how their structure changes with processing [1]. Many modern characterisation techniques such as XRD, differential scanning calorimetry (DSC), DTA, FTIR, Raman spectroscopy, nuclear magnetic resonance (NMR), energy dispersive X-ray analysis, (EDX) and others have been widely recommended and used for this purpose [2-4]. The investigation of the amorphous and crystallisation regions of chalcogenide glasses is of practical interest for obtaining new materials with semiconducting properties [5]. It is also of theoretical interest to acquire knowledge for the basic understanding of certain mechanisms and possible deposition methods for large-scale productions. In earlier studies [6-8], the mole % of Sn in Ge_{1-x}-Sn_x-Se_2, As_{33}-$Se_{67-x}Sn_x$ and Ge-Sn-Sb-Se was found to be 19.8, 7.0, and 12.5%, respectively in the glass formation region. Introduction of Sn into the Sn-Sb-Se system, with 4 co-ordination numbers before the stoichiometirc compound, was assumed and expected to be incorporated in the glass formation of up to 12.5 Sn-mole % [9-11]. However, above this range, increasing Sn% was expected to increase the difficulty of glass formation due to the chemical properties and the distinct metallic character of Sn with 6 co-ordination numbers [12-15]. In this work, the structural state, IR and Raman analyses and glass transition temperature, have been investigated in order to elucidate the characteristic properties of the Sn_x-Sb_{15}-Se_{85-x} system.

2 Experimental procedure

Granules of Sn and Sb having 99.999% purity and that of Se, 99.99% were used. The containers in which these materials were stored were opened in a controlled way to minimise contamination. A 5.00 g sample was batched in a closed scale balance on which Sn, Sb, and Se were weighted using sample percentage procedures [10]. Batched elements were placed in a pre-cleaned quartz ampoule. The ampoule was attached to the vacuum pump and evacuated to 66.5 Pa. Then an inert argon gas was supplied for half an hour while pumping continued. The ampoule was later sealed using an oxygen-natural gas flame melt by heating its wall, bending it carefully and sealing it up. Selenium is recognised to have high vapour pressure and also has the tendency to react with oxygen. Thus, care and precaution were taken to avoid any explosion during the sealing of the tube. Then the ampoule was transferred into a specially designed orbital-shaking furnace. A heating cycle of up to 700°C for 6 hours was applied at a rate of 5°C per minute. In order to prepare homogenous samples, agitation of 100.0 rotations per minute (rpm) was applied using an attached orbital shaker. The ampoule was dropped in liquid nitrogen for the fast cooling requirement. XRD (Siemens-Diffractometer D-5000) was performed on fine powders of as-prepared samples using 40 kV energy, 30 mA current, CuKa-radiation (λ =1.5418 Å) with a resolution of 0.04°/m in the range of 2 to 60° and scanning mode of 2θ. Glass transition temperature T_g, was obtained using DTA (Perkin Elmer-538N/3021903) with a matched pair of thermocouples constructed from platinum

and platinum/10% rhodium. A sample of 10 mg was run in DTA7 at a heating rate of 10 °/min. The transmission spectra (FTIR Shimadzu- spectrophotometer 8000) were obtained at room temperature in the spectral range 300-100 cm-1 and 2.0 cm-1 resolution. Polarised Raman spectrum (Magna-spectrometer 560) was recorded in the range 400-100 cm-1 with 4 cm-1 step at room temperature, on a KBr technique prepared disc using a near 90° scattering configuration. The number of photons counted at each step was stored in a computer.

3 Results and discussion

3.1 XRD-results

The XRD of the Sn_x-Sb_{15}-Se_{85-x} system, where x = 0, 5, 10, 12.5, showed an amorphous state, as indicated by a series of broad plateau and intermittent small peaks of background noise in Fig. 1. The XRD spectrum of x = 15-mole % showed crystalline structure. For more details of the crystalline structure of this sample and other samples of Sn-Sb-Se system, interested readers can refer to ref. [11]. As shown in Table 1, the sample x = 15-mole % represents the maximum domination of fraction of Sn-Se bond compared to that Sb-Se bond in Sn-Sb-Se system [9]. It was mentioned that Sn, Sb, and Se in their binary stoichiometric Sb_2Se_3 and $SnSe_2$ were co-ordinated with 6 and 5, resulting in Se co-ordination change from 2 to 3. Their corresponding average co-ordination numbers were μ = 3.8 and 4.0, respectively, which were more than μ = 3, which is Philips'

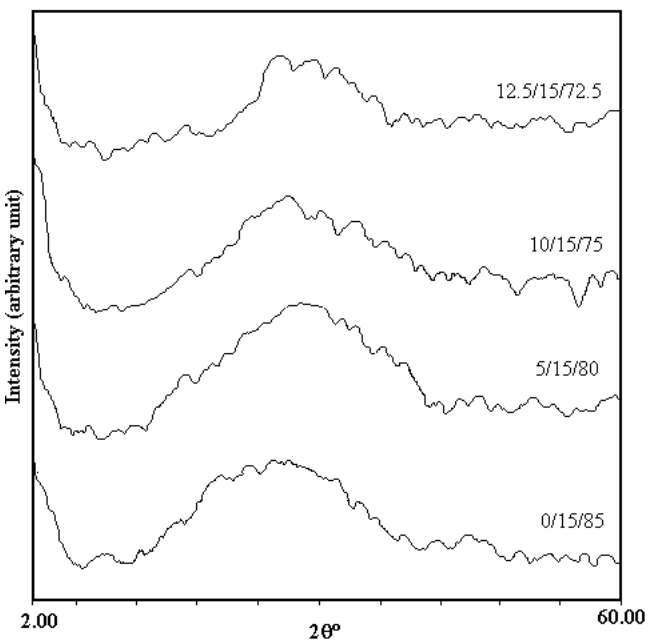

Figure 1: XRD-result on amorphous samples of Sn_x-Sb_{15}-Se_{85-x} where x = 0, 5, 10 and 12.5.

Table 1: The bond fractions and average co-ordination number, μ, that calculated for Sn_x-Sb_{15}-Se_{85-x} system according to [9] and the glass transition temperature, T_g.

Sample	$f_{Sn\text{-}Se}$ %	$f_{Sb\text{-}Se}$ %	$f_{Se\text{-}Se}$ %	μ	T_g (°C)
0/15/85	0.0	41.9	58.1	2.2	161.0
5/15/80	17.8	40.0	42.2	2.3	139.2
10/15/75	34.0	38.3	27.7	2.4	128.0
12.5/15/72.5	41.7	37.5	20.8	2.4	121.6
15/15/70	49.0	36.7	14.3	2.5	Crystalline
14.3/28.7/51	44.5	66.9	-11.4	2.6	Crystalline

maximum glass formation condition [3, 5]. In order to fulfil this condition, it was restricted that the coordination numbers of Sn, Sb, and Se in the amorphous region always remain as 4, 3 and 2, respectively, and this ruled out their stoichiometric compositions' coordination numbers [9]. Thus, the glass formation region of the Sn-Sb-Se system was arrested between the average coordination number, $\mu \leq 2.4$ and the fraction of Sn-Se bonds, $f_{Sn\text{-}Se} < 44.5\%$. XRD proved that the amorphous state of Sn_x-Sb_{15}-Se_{85-x} the system occurred within the arrested region.

3.2 FTIR spectra

Figure 2 shows the infrared spectra of the Sn_x-Sb_{15}-Se_{85-x} system (where x = 5, 10 and 15). The infrared transmission (%) versus the wave number (cm^{-1}) in the bottom spectrum shows four transmission bands. The band between 122 and 145 cm^{-1} is assigned to tetrahedral $SnSe_4$ mode. A 150 cm^{-1} vibrational frequency was calculated and assigned to tetrahedral double bond $SnSe_4$ stretching mode, using Somayajulu's method [10, 16]. This band may also be assigned to the Se_8-ring bending mode, whereas a-115 cm^{-1} band was assigned to the Se_8 chain in Ge-Se alloy [17]. However, the extended band between 170-145 cm^{-1} is attributed to the $SbSe_3$ bending mode as reported by Kato, et al. [18]. Its shoulder at 159 cm^{-1} is assigned to the $SnSe_4$ bending mode. In addition to this, the band situated between 176-208 cm^{-1} is ascribed to $SbSe_3$ stretching mode, whereas the shoulder at 186 cm^{-1} shows another $SbSe_3$ bending mode. Sharma et al. [19] also mentioned similar band formation. The band with high intensity peak ranging 208-250 cm^{-1} is for the Se_8 stretching mode. Goyal and Mann [17] assigned the absorption peaks around 227 and 247 cm^{-1} to the Se-polymeric chain and Se_8 ring mode, respectively.

The second spectrum is for Sn = 10-mole % sample. A new band ranging 100-120 cm^{-1} is assigned to the tetrahedral $SnSe_4$ mode. On the other hand, the band ranging 120-152 cm^{-1} is ascribed to the tetrahedral $SnSe_4$ bending mode. However, a series of shoulders occurred between 152-196 cm^{-1}, and those extended between 152-169 cm^{-1} and 177-187 cm^{-1} are assigned to the $SnSe_4$ bending mode and the $SbSe_3$ stretching mode, respectively. Meanwhile, the rest

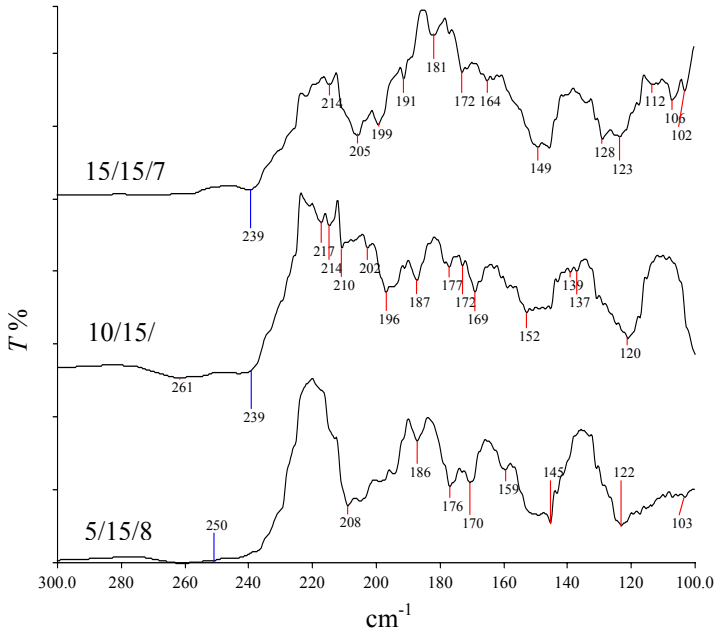

Figure 2: Infrared spectra of the Sn_x-Sb_{15}-Se_{85-x} system.

of shoulders are ascribed to the $SbSe_3$ bending mode. The other band of this spectrum, which extends between 196-239 cm^{-1} with shoulders at 202, 210, 214 and 217 cm^{-1} are assigned to the Se_8 chain and Se-Se bending mode, respectively.

The domination of Sn-concentration has clearly modified the infrared spectrum in Sn = 15-mole% by causing high intensity and a wide band peak between 149-205 cm^{-1}, which was not observed in the preceding spectra. This band can be divided into two regions between 149-172 cm^{-1} and 172-191 cm^{-1}, which are assigned to the $SnSe_4$ and $SbSe_3$ stretching modes, respectively. On the other hand, the shoulders at 164, 181 cm^{-1} and that at 199 cm^{-1} are ascribed to the $SnSe_4$ and $SbSe_3$ bending modes, respectively. Furthermore, the band between 205 and 239 cm^{-1} with a shoulder at 214 cm^{-1} is attributed to Se-Se stretching and the Se_8 chain modes, respectively. As shown in Table 1, the fraction of Sn-Se bond is 49%, while that of Sb-Se and Se-Se bonds are 36.7 and 14.3%, respectively. This sample showed a crystalline phase of $Sn_2Sb_4Se_8$ [10-11]. This phase might give rise to a new feature band at 149-205 cm^{-1}. However, the band around 102-123 cm^{-1} and 128-149 cm^{-1} is ascribed to the $SnSe_4$ bending mode.

3.3 Raman spectra

The Raman spectra of Sn_x-Sb_{15}-Se_{85-x} system are shown in Fig. 3. A peak of 250 cm^{-1} dominates the Raman spectrum of amorphous Se. This peak was also a characteristic of monoclinic selenium [20]. The Raman peak at 250 cm^{-1} was

therefore assigned totally to the symmetric vibration mode of the Se_8 ring based on this evidence and the fact that this line is polarisation dependent. The weak shoulder at 239 cm^{-1} was observed in amorphous Se, which coincided with a dominant peak of crystalline trigonal Se [20]. Hence, the low frequency band at 239 cm^{-1} is assigned to the Se_8-bending mode. On the other hand, Raman vibrations at 235 cm^{-1} and 255 cm^{-1} were assigned for Se-Se chain in Ge_xSe_{1-x} glasses [21].

It is noticeable that the Raman intensity at 250 cm^{-1} is lowered and assigned to the Se_8 bending mode in Sn_5-Sb_{15}-Se_{80} spectrum. A wide band peak that occurs around 190 cm^{-1} is assigned to the $SbSe_3$ stretching mode. The shoulder observed at 153 cm^{-1} is attributed to the $SnSe_4$ bending mode. Raman spectrum of $Sn_{10}Sb_{15}Se_{75}$ showed that the peak shifted at 190 cm^{-1} with a more increased intensity than that of Sn = 5-mole %. This peak was not found in the preceding spectra probably because of Sn that enters the chain with 4-co ordination and resulting in $f_{Sn\text{-}Se}$ = 34.0. This almost equals to (1/3x100) the $f_{Sn\text{-}Se}$ in stoichiometric $SnSe_2$ and similar to that of $f_{Sb\text{-}Se}$ = 38.0%, as shown in Table 1. Thus, it is reasonable to assign this peak to a symmetrical vibration of $SnSe_4$ stretching mode. Therefore, the rest of selenium atoms consequently caused the formation of the Se chain as indicated by the vibration peak at 260.0 cm^{-1}.

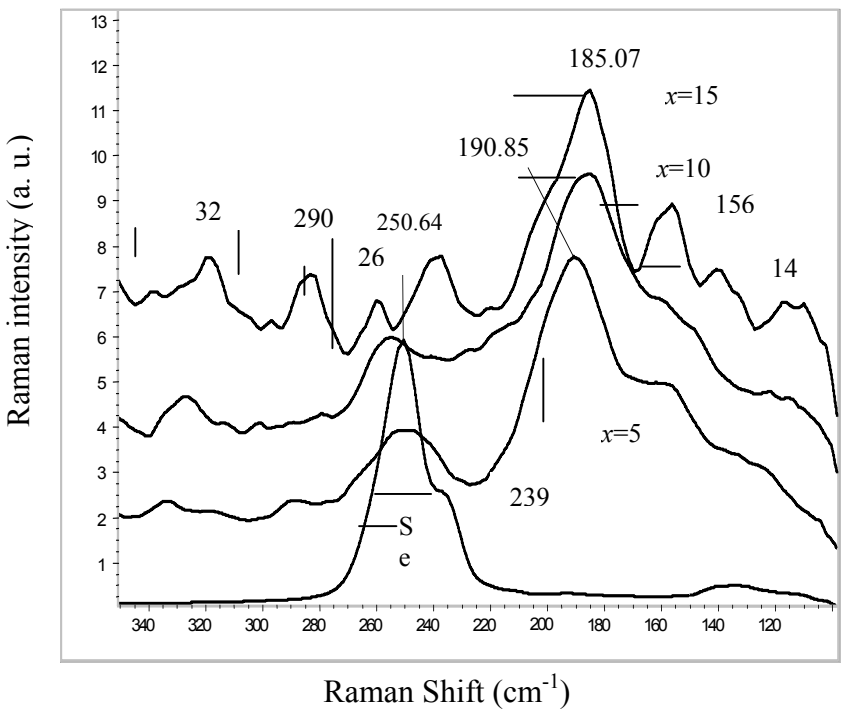

Figure 3: Raman Spectra of the amorphous Se and Sn_x-Sb_{15}-Se_{85-x} system, (x = 5, 10 and 15).

As for the ternary $Sn_{15}Sb_{15}Se_{75}$ crystalline sample, the Raman spectrum shows a change in the position and intensity of the peak that is mostly related to the large amount of Sn-Se bonds. Two peaks of this spectrum are observed at 153 cm $^{-1}$ and 185 cm^{-1}. In this spectrum, the vibration of $SnSe_4$ unit is less pronounced than that of $SnSe_2$ unit. However, Raman shift at 189 cm^{-1} was assigned to $Sn(Se_4)_{1/2}$ units in $Ge_{1-x}Sn_xSe_2$ alloy glasses [22]. This is presumably due to the presence of short selenium chains between the two tetrahedrals, which in turn missed the vibration mode at 250 cm^{-1}. However, the intensity of the peak at 239 cm^{-1} is higher and in a slightly different manner compared to the previous samples. This difference in peak intensity can be explained using $f_{Sn\text{-}Se}$ = 49.0% and $f_{Se\text{-}Se}$ = 14.3% as shown in Table 1. It means that all Sn and Sb atoms are bonded to four and three Se atoms, respectively, while the rest of Se atoms causes Raman peak at 239 cm^{-1}. Further bands are observed around 140 and 156 cm^{-1}, which are attributed to the symmetrical bending mode of $SnSe_4$ and $SbSe_3$, respectively. Also, weak peak bands are located around 265, 290 and 320 cm^{-1}. The band around 265 is assigned to the Se_8 bending mode. The rest of the bands might be ascribed to ternary crystalline phase $Sn_2Sb_4Se_8$, which was identified from XRD analysis of this sample in [11].

The IR and Raman spectroscopy results help explain the structure of Sn-Sb-Se system. The addition of Sn-mole % to the system modifies the Sb-Se structure and incorporates with the 4-co-ordination number in glass region. The observation of Se stretching bond supports the glass formation in Se-rich region at which the Sn and Sb mole % are less than their stoichiometric binary compounds with Se. The structure of Sn-Se and Sb-Se glasses can be envisaged as the local co-ordination that satisfies the 8-N rule of the classical valence bond theory [23-25]. The structure of Se glasses was believed to consist of long chains of selenium atoms, each having a co-ordination number of 2 [20]. To these selenium chains, small amounts of cross-linking atoms, such as Sn and Sb, were added. These amounts should be less than that required for $SnSe_2$ and Sb_2Se_3 stoichiometric compositions. Consequently, the glass structure can build up as follows: Sn atoms are 4 co-ordinated when covalently bonded, and each Sn atom having bonds to Se atoms, while Sb atoms are 3 co-ordinated and each Sb atom having bonds to Se atoms. It was deduced that the basic structural unit of $SnSe_2$ glass was made of $SnSe_4$ tetrahedral and that of Sb_2Se_3 glass was made of $SbSe_3$ pyramidal. These units spread out among Se chains and form a net of Se_3-Sn-Se-Se-Sb-Se_2 glass structure [10]. The occurrence of a new IR transmission band around 125-145 cm^{-1} and the shift of Raman peak from 190 cm^{-1} to 183 cm^{-1}, which happen due to the increase of Sn mole % when Sb-mole% fixed at 15, is a strong evidence that supports the configuration of this net structure.

3.4 DTA result

Figure 4 illustrates the DTA-temperature (°C) plots against dT as a function of changing Sn-mole % in Sn_x-Sb_{15}-Se_{85-x} system, with x = 0, 5, 10 and 15-mole %. A curve of composition Sb_{15}-Se_{85} shows the glass transition temperature, T_g, at 161.0 °C and the onset crystallisation temperature, T_c, at 219.0 °C, while the

endothermic peak temperature, T_p, occurs at 234.0 °C. Fast reduction in T_g to 139.2 °C is observed due to the addition of Sn = 5-mole % as shown in $Sn_5Sb_{15}Se_{80}$ curve. Likewise T_c and T_p are reduced to 212.7 °C and 224.4 °C, respectively.

The behaviour of the curve is changed for Sn = 10-mole % as shown in the third one from the bottom. The T_g is reduced to 128 °C, while T_c occurred at 215.4 °C and T_p is observed at 225.7 °C. Lastly, the upper curve is for the crystalline $Sn_{15}Sb_{15}Se_{70}$. In this curve T_g disappeared, while T_c and T_p occurred at 329.8 and 378.5 °C, respectively. This analysis supports the XRD result that showed crystalline structure of this sample in [11].

The DTA data clearly revealed that alloying of Sn, Sb, and Se in Sn_x-Sb_{15}-Se_{85-x} system showed a continuous decrease in T_g by increasing Sn content from 0 to 10-mole% as shown in Figure 4. Increasing the Sn-mole % in large concentration completely modified the structure of the network. It should be mentioned that for Sn = 0, 5 and 10-mole %, the samples were found in amorphous state and turned into crystalline structure at Sn = 15 -mole % from XRD-analysis. However, it appeared that to induce chemical modification in the host network, the incorporation of Sn and Sb with 4 and 3 coordination numbers were the best requirements to fit the glass formation.

It is observed from the figure that a marked change in T_c at Sn = 10-mole % can be explained in different approaches. Feltz [15] stated that, 'an exothermic enthalpy effect is observed if the heating rate falls below the cooling rate. The system, approaching the T_g region with a decrease in volume or by release of enthalpy, is transformed to a super cooled melt.

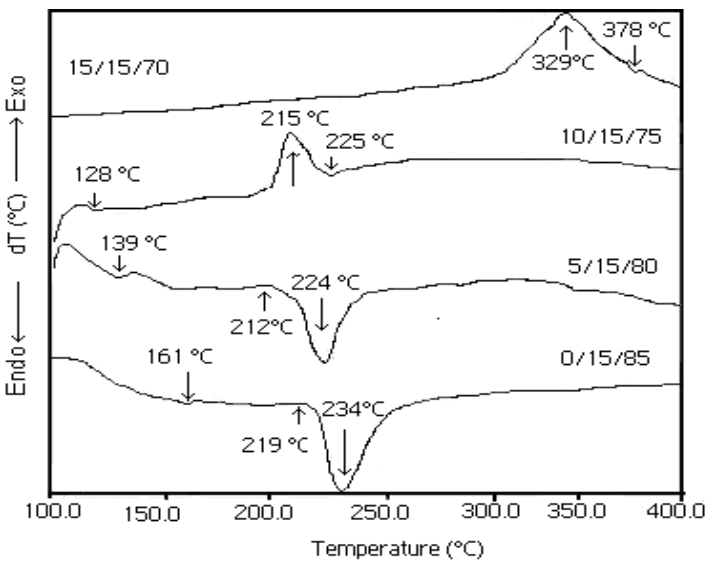

Figure 4: Change in T_g, T_c and T_p from DTA curves as s function of Sn mole % for Sn_x-Sb_{15}-Se_{85-x} systems, where x = 0, 5, 10 and 15, respectively.

However, Fouad et al. [26] reported the appearance of double glass transition temperature as an indication of the retention in a quenched sample of two truly amorphous phases. It might be due to the network of the present glassy system that changes from being mechanically floppy to rigid, or there is a change in the network dimensionality from a one-dimension (1D) to a two-dimension (2D) network (Philip-Thorpe rigidity transition). It was clearly seen from XRD that the $SnSe_2$ and Sb_2Se_3 crystalline phases were found in Sn = 15-mole % [11]. Thus, the structure of Sn = 10-mole % might be approaching the verge of crystalline stage and Phillips' threshold. However, for this sample μ = 2.4 the maximum condition of Sb to be amorphous with Se, with 3 and 2 coordination numbers and $f_{Sn\text{-}Se}$ = 34%, which is approximately equal to (1/3x100) the fraction of $f_{Sn\text{-}Se}$ in stoichiometirc $SnSe_2$. The $f_{Sn\text{-}Se}$ = 100% for stoichiometirc $SnSe_2$ [10]. The observed behaviour in T_g and T_c can be interpreted by using the chemical ordered network (CON) model [9] by considering the chemical bond energy. The coordination number of individual elements satisfies six types of bonds using Pauling's method, namely, Se-Se: 44.0 kcal/mol, Sn-Se; 47.4 kcal/mol, Sb-Se: 42.9 kcal/mol, Sn-Sn: 34.2 kcal/mol, Sb-Sb: 30.2 kcal/mol and Sn-Sb: 32.43 kcal/mol [10]. Therefore, the observed continuous decrease in the value of T_g in the amorphous samples might be due to Sn that shared and replaced Sb in the Se-Sb-Se_2 bonds, which takes a form of Se-Sb-Se-Sn bonds. In the binary Sb_{15}-Se_{85} sample, the Sb-Se bond is stronger, thus the T_c is higher when Sn is added due its high bond energy that starts gradually to replace the location of Sb, but its content is not enough to form a complete $SnSe_4$ bonds. Thus, T_g decreases by increasing the dislocation of Sb until the Sn-atoms find their comfortable position and form SnSe4 bond that is not shared with Sb. As reported in [11], the first crystalline peak of the sample $Sn_{7.5}Se_{92.5}$ was a crystalline $SnSe_2$ and not $SnSe_4$, which indicated that the coordination numbers of Sn and Se were 6 and 3, respectively, and not 4 and 2 as usual. Thus crystalline $SnSe_2$ is formed. In order to melt it, a high temperature is required. Meanwhile, the Se-Se bonds are not enough to satisfy the Sn-6-codinatinon numbers of crystalline phases SnSe and $SnSe_2$. When Sn = 15, the occurrence of stronger $SnSe_2$ bonds appeared, and the Sn-6-coordination numbers cause the Se coordination number to increase from 2 to 3, resulting in the overlapping of T_g and T_c at 325 °C.

4 Conclusion

It is concluded that the alloying of Sn, Sb, and Se elements in the Sn_x-Sb_{15}-Se_{85-x} system showed the amorphous state of Sn-mole % to be equal to 0, 5, 10, and 12.5. IR-transmission indicates that for the amorphous sample, asymmetrical stretching of the pyramidal $SbSe_3$ mode is dominant around 190 and 210 cm^{-1}. Se-chain bands occur around 210-239 cm^{-1}. Addition of Sn-mole % to the binary system showed shifting of the peaks and occurrence of a new transmission band around 125-145 cm^{-1}. This band is ascribed to the asymmetrical infrared active of the tetrahedral $SnSe_4$ mode. Raman spectrum for pyramidal $SbSe_3$ occurred at 190 cm-1, while the addition of Sn mole % increases the peak intensity and causes the Raman shift towards 183 cm^{-1}, indicating the formation of Sn-Se

bonds. DTA revealed that the glass transition temperature decreased with increasing Sn-mole % in the amorphous samples and completely disappeared in the crystalline samples.

References

[1] Wallidge, G. W., Adnderson, R., Mountjoy, G., Pickup, D. M., Gunawidjaja, P., Newport, R. J. and Smith, M. E. J. of Mat. Sc. **39,** 6743, 2004.
[2] Hosokawa, S. and Tamura, K. J. Phys.: Condens. Matter. 16 (2004) 1465.
[3] Page, T. F. and Shaw, B. A. J. of Mat. Sc. **39,** 6791, 2004.
[4] Chapman, L. A. J. of Mat. Sc. **39,** 7229, 2004.
[5] Hilton, A. R. and Jones, C. E. Phys. and Chem. of Glasses, **7(4),** 112, 1966.
[6] Kislitskaya, E. A. and Kokorina, V. F. Zhur. Prik. Khimii. **44(3),** 646, 1971.
[7] Mikrut, J. M. and McNeil, L. E. J.of Non-crystalline Solids. **114,** 127, 1989.
[8] Jagatap, S. R., and Zope, J. K. J. of Non-Crystalline Solids. **127**, 19, 1991.
[9] Adam, A. B., Sakrani, S. and Wahab, Y. J. of Mat. Science. **40(7),** 1571, 2005.
[10] Adam, A. B. PhD-Thesis. University of Technology, Malaysia. 2002.
[11] Adam, A. B., Sakrani, S. and Wahab, Y. J. Mater Sci. **41**, 5797-5801, 2006.
[12] Philips, J. C. J. of Non-crystalline solids. **34,** 153, 1979.
[13] Chelikowsky, J. R. and Philips, J. C. Physical Review B. **17(6),** 2453, 1978.
[14] Zhenhua, L. Journal of Non-Crystalline Solids. **127**, 298 1991.
[15] Feltz, A. Amorphous Inorganic Materials and Glasses. Weinheim, N. York, Tokyo; VCH. 1993.
[16] Somayajulu, G. R. J. of Chemical Physics. **28(5),** 814 1958.
[17] Goyal, D. R and Mann, A. S. J.of Non-crystalline Solids, **183,** 182, 1995.
[18] Kato, M., Onari, S. and Arai, T. Jap. J. of Appl. Phys. **22(9),** 1382 1983.
[19] Sharma, A. k., Bhatia, K. L., Bhatnagar, V. K and Malik, S. K. J. of Non-crystalline Solids. **108,** 309, 1989.
[20] Mort, J. "Raman Spectroscopy". In Electronic and structural properties of amorphous semiconductors. (ed.) Le Comber, P. G. and Mort, J. London & New York; Academic Press. 475, 1973.
[21] Wong, Y., Matsuda, O., Inove, K., Yamamuro, O., Matsuo, T. and Murose, K. Journal of Non-Crystalline Solids, **232–234,** 702, 1998.
[22] Stevens, M., Boolchand, P. and Hernandez, J. G. Phys. Review B. **31(2**), 981, 1985.
[23] Giridhar, A., Narasimham, P. and Mahadevan, S. J. of Non-crystalline Solids **37**, 165, 1980.
[24] Mukherjee, A. K., Dhawan, U., Kundra, K. D., Mondal, M. and Ali, S. Z. Indian J. of Pure and Applied Physics. **20**, 681, 1982.
[25] Aronovitz, J. A., Bonavar, J. R., Marcus, M. A. and Phillips, J. C. Physical Review B. **28(8),** 4454, 1983.
[26] Fouad, S. S., Fayek, S. A. and Ali, M. H. Vacuum. **49**, 25, 1998.